MATERIALS SCIENCE

Intrinsically disordered proteins access a range of hysteretic phase separation behaviors

Felipe Garcia Quiroz[1]*, Nan K. Li[2†], Stefan Roberts[1], Patrick Weber[3], Michael Dzuricky[1], Isaac Weitzhandler[1], Yaroslava G. Yingling[2], Ashutosh Chilkoti[1‡]

The phase separation behavior of intrinsically disordered proteins (IDPs) is thought of as analogous to that of polymers that undergo equilibrium lower or upper critical solution temperature (LCST and UCST, respectively) phase transition. This view, however, ignores possible nonequilibrium properties of protein assemblies. Here, by studying IDP polymers (IDPPs) composed of repeat motifs that encode LCST or UCST phase behavior, we discovered that IDPs can access a wide spectrum of nonequilibrium, hysteretic phase behaviors. Experimentally and through simulations, we show that hysteresis in IDPPs is tunable and that it emerges through increasingly stable interchain interactions in the insoluble phase. To explore the utility of hysteretic IDPPs, we engineer self-assembling nanostructures with tunable stability. These findings shine light on the rich phase separation behavior of IDPs and illustrate hysteresis as a design parameter to program nonequilibrium phase behavior in self-assembling materials.

INTRODUCTION

Stimuli-responsive polymers that undergo equilibrium, aqueous phase separation in response to environmental stimuli have driven innovations in nanotechnology (*1*), drug delivery (*2*), tissue engineering (*3*), regenerative medicine (*4*, *5*), and biotechnology (*6*, *7*). More recently, the discovery that intrinsically disordered proteins (IDPs) in nature also undergo aqueous phase separation in the cell has led to intense interest in understanding their phase separation behavior (*8*, *9*). Progress in this understanding promises to advance biology and deliver tools to engineer advanced protein-based materials (*10*, *11*).

Polymers and IDPs that exhibit liquid-liquid phase separation belong to one of two classes: They exhibit lower critical solution temperature (LCST) or upper critical solution temperature (UCST) phase behavior (*10*, *12*); and a smaller subset exhibit both behaviors (*12*, *13*) . For polymers that exhibit LCST phase behavior, below a critical temperature—the cloud point temperature (T_{cp})—the polymer is miscible with water and is hence soluble, while at temperatures above the T_{cp}, phase separation occurs to create two immiscible phases that exist in thermodynamic equilibrium—a polymer-rich phase and a dilute phase of soluble polymer in water. UCST phase behavior is the mirror image of LCST phase behavior, so that phase separation occurs upon cooling below the T_{cp}. With few exceptions (*14*, *15*), well-studied LCST and UCST polymers show negligible thermal hysteresis in their phase separation behavior (*16*–*19*), in that the temperature at which they cross the phase boundary is nearly independent of the direction (heating or cooling). As a result, hysteresis and nonequilibrium properties in the aqueous phase behavior of polymers have been largely ignored as a design parameter to program phase separation–driven assembly (*5*).

We hypothesized that because nonequilibrium properties are common to protein assemblies (*8*), the phase separation behavior of IDPs was unlikely to follow the equilibrium behavior of synthetic polymers and could potentially access nonequilibrium or hysteretic states upon phase separation. Motivated by the desire to dissect and use the nonequilibrium and kinetic properties of phase-separated protein assemblies, here, we probe the largest extant library of LCST- and UCST-exhibiting IDP polymers (IDPPs) (*10*) to uncover unique features of the phase separation behavior of IDPs.

Through experiments and simulations, we discovered a wide range of distinct hysteretic phase behaviors in IDPPs, wherein stable peptide-peptide—hydrophobic and hydrogen bonding—interactions in the aggregated state counter chain disentanglement and kinetically trap the insoluble polymer phase at temperatures well past their expected disaggregation temperature. We show that hysteresis can be encoded and tuned at the repeat level by syntax—the precise position of an amino acid within a repeat—and at the macromolecule level through chain length. Last, we exploit hysteresis as a previously unidentified variable that is complementary to amphiphilicity to control the assembly of diblock IDPPs into highly stable nanoparticles that resist thermally triggered disassembly. We suggest that unraveling the sequence-level determinants of nonequilibrium phase behavior in protein polymers will enable innovations in bottom-up self-assembly of biomaterials (*20*–*22*) and provide insights into the phase behavior of IDP assemblies in biology (*8*, *23*).

[1]Department of Biomedical Engineering, Duke University, Durham, NC 27708, USA. [2]Department of Materials Science and Engineering, North Carolina State University, 911 Partners Way, Raleigh, NC 27695, USA. [3]Swiss Nanoscience Institute, University of Basel, Klingelbergstrasse 82, 4056 Basel, Switzerland.
*Present address: Howard Hughes Medical Institute, Robin Chemers Neustein Laboratory of Mammalian Cell Biology and Development, The Rockefeller University, New York, New York 10065, USA.
†Present address: Molecular Foundry, Lawrence Berkeley National Laboratory, 1 Cyclotron Rd, Berkeley, CA 94720, USA.
‡Corresponding author. Email: chilkoti@duke.edu

RESULTS AND DISCUSSION

IDPPs access a wide range of hysteretic phase behaviors

To investigate nonequilibrium phase behaviors in IDPs, we synthesized and characterized IDPPs by optical turbidity measurements [at 50 μM in phosphate-buffered saline (PBS)] over two to three cycles of heating and cooling (both at 1°C/min) around their critical cloud point temperatures. The studied IDPPs are composed of recently identified diverse repeat motifs that encode LCST or UCST

phase behavior (*10*). We first examined the reversibility of the phase behavior of IDPPs resulting from all 24 LCST motifs in our library. To assess thermal hysteresis, we operationally defined it as the absolute difference between the T_{cp} (inflection point on optical turbidity as a function of temperature) observed at the onset of phase separation on heating and the apparent T_{cp} upon dissolution of the phase-separated, IDPP-rich droplets on cooling.

This approach revealed three types of phase behavior among LCST IDPPs that are defined by the degree of thermal hysteresis: (i) negligible (~0°C), (ii) moderate (10° to 30°C), and (iii) large (>40°C), environmentally sensitive hysteresis (Fig. 1A). In the first group, similar to canonical LCST-exhibiting polymers such as elastin-like polypeptides (ELPs), we observed negligible thermal hysteresis. The second group displayed reproducible and sizable degrees of thermal hysteresis (Fig. 1B). Unexpectedly, some IDPPs (group iii) that showed large hysteresis—admittedly irreversible—in our initial experimental conditions showed moderate or negligible hysteresis when phase separation was triggered at lower temperatures in PBS supplemented with NaCl (Fig. 1C), showing that these IDPPs can also exhibit fully reversible LCST phase behavior. Notably, most of the group iii IDPPs display zero hysteresis if their cloud point is triggered below a critical threshold temperature—typically around 40°C—by the addition of 1 M NaCl (fig. S1). In contrast, group iii IDPPs undergo a sharp and nearly irreversible phase transition in PBS or PBS with additional salt (1 M NaCl) when heated above this threshold, as shown by the lack of reversibility in their turbidity versus temperature profile, despite prolonged undercooling (Fig. 1C and fig. S1G).

To explore the role of IDPP chain length on the degree of thermal hysteresis, we synthesized polymers with a VAPVG repeat unit, a motif in our library that when polymerized encoded moderate hysteresis (Fig. 1A), with stepwise increases in the number of repeat units and characterized them over a range of cooling rates. We found that hysteresis increases with the chain length (Fig. 1D and fig. S2A) and that a minimum number of repeats (~40 for VAPVG) is required to exhibit pronounced hysteretic behavior, as seen by a sharp transition on cooling (i.e., a well-defined inflection point) that is largely insensitive to cooling rate (Fig. 1E). This minimal chain length can be further decreased if IDPPs are designed to include a multimerization domain, which is a common architectural feature in native

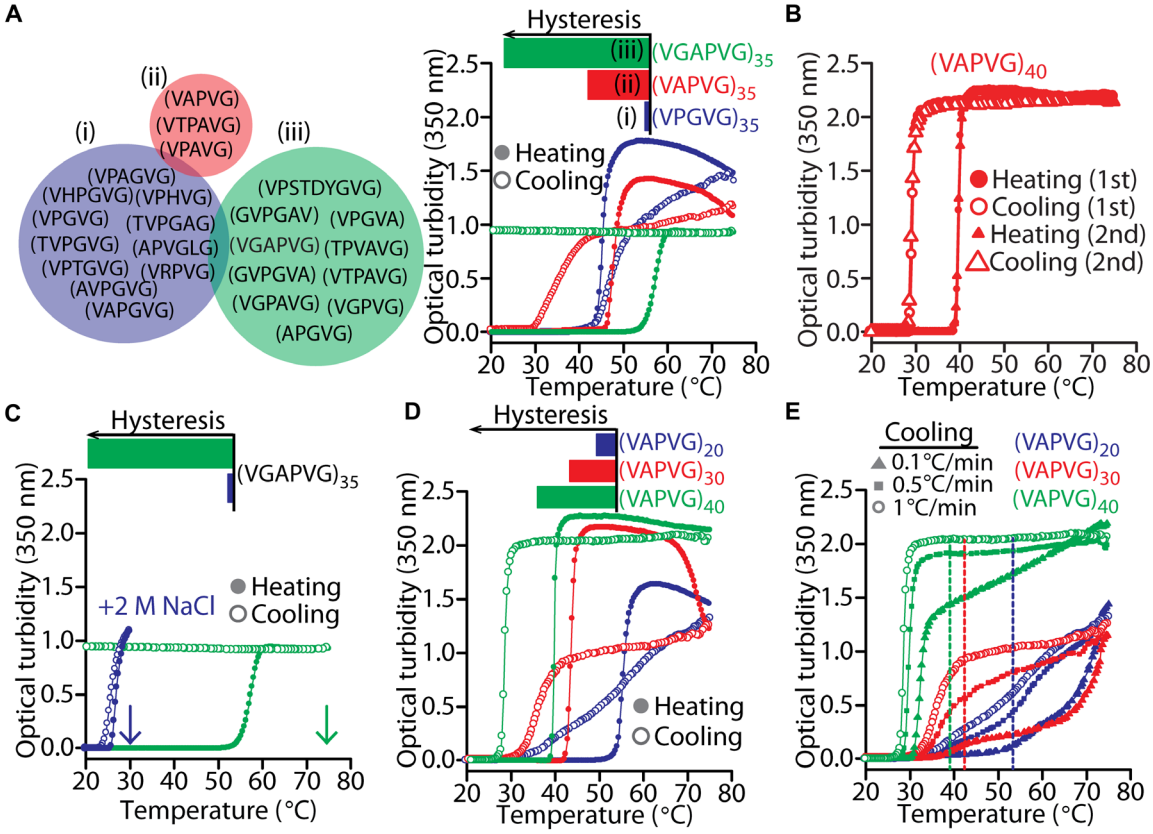

Fig. 1. LCST IDPPs exhibit a wide range of hysteretic phase behaviors. (**A**) Analysis of the reversible phase behavior of LCST IDPPs in our library revealed three groups of repeat motifs, wherein motifs in each group encode one of three types of phase behavior characterized by differences in the degree of thermal hysteresis seen on cooling below the cloud point temperature, ranging from (i) negligible (~0°C) and (ii) moderate (10° to 30°C) to (iii) large, environmentally sensitive hysteresis. Here, we show temperature-dependent optical turbidity over a full cycle of heating and cooling pass the T_{cp} for three representative IDPPs that exhibit the full range of observed hysteretic behaviors. As a guide to the eye, each panel includes a legend with a qualitative indicator of the degree of hysteresis for each repeat motif. (**B**) IDPPs made of (VAPVG) repeats exhibit highly reproducible degrees of thermal hysteresis over multiple cycles of phase separation. (**C**) Extension of data in (A) examining the phase behavior of $(VGAPVG)_{35}$ to show its large, environmentally sensitive hysteresis, as it shows (in separate experiments) large or negligible thermal hysteresis depending on the maximum temperature (shown by arrows) reached during the heating part of the cycle. (**D**) Hysteretic phase behavior of IDPPs with an increasing number of (VAPVG) repeats. (**E**) Analysis of IDPPs in (D) but varying the cooling rate (from 1° to 0.1°C/min). To improve data visualization, the corresponding T_{cp} on heating are shown as vertical dashed lines. All optical turbidity measurements were performed at a fixed concentration of 50 μM in PBS, with heating and cooling at 1°C/min, unless otherwise stated.

IDPs (fig. S2B shows the pronounced hysteretic behavior for 20 repeats of VAPVG when fused to a trimerization domain). Increasing the number of repeats in IDPPs with negligible hysteresis did not lead to the emergence of hysteretic phase behavior (fig. S2C).

We then examined the reversible phase behavior of UCST IDPPs in our library (*10*). UCST IDPPs did not display the range of hysteretic behaviors observed for LCST IDPPs. Instead, either they phase separated fully reversibly over multiple cycles of cooling and heating or they rapidly underwent progressive loss of reversibility (fig. S3), as has also been observed in synthetic polymers that exhibit UCST behavior (*24*). Unlike the reproducible hysteretic phase behavior of LCST IDPPs, UCST IDPPs often show a progressive build-up of aggregates, reminiscent of the phase behavior recently observed for low complexity, disordered domains of RNA-binding proteins (*25*, *26*). However, we note that, analogous to the behavior of LCST IDPPs, the progressive "aging" of UCST IDPP aggregates is exacerbated by increases in their number of repeats (fig. S3B).

Molecular origins of thermal hysteresis in IDPPs

Protein polymers composed of a noncanonical elastin-like motif, VPAVG, have been reported to exhibit moderate degrees of thermal hysteresis (*15*, *27*). The mechanism behind this hysteretic behavior has been suggested to arise from the disruption of the PG dipeptide that is critical for β-turn formation, although other β-turn structures involving other residues may still occur (*15*). In our library of LCST IDPPs, however, circular dichroism (CD) spectroscopy showed that at temperatures below the T_{cp}, both nonhysteretic and hysteretic IDPPs shared a similar conformational signature that is characteristic of IDPs (fig. S4). This observation suggested that emergence or disruption of specific structural motifs is unlikely to drive hysteretic phase behavior.

We next performed CD spectroscopy on IDPPs as a function of solution temperature to further probe the structural origins of hysteresis (Fig. 2). First, by measuring CD spectra of IDPPs before, during, and after their onset of aggregation, we show that IDPPs exhibit minor changes in conformation at the T_{cp}—mainly a small decrease in the intensity of the negative peak at ~197 nm that is indicative of a random coil—but undergo a significant change in their CD spectra well above the T_{cp}, as typically seen by a large decrease in the intensity of the negative peak at ~197 nm (Fig. 2). For polymers with a negligible to moderate degree of hysteresis in their LCST behavior, upon cooling below their T_{cp} (as defined by the degree of thermal hysteresis), their CD spectra revert back to the profile seen before heating the sample (Fig. 2, A and B). In contrast, for IDPPs that exhibit a large degree of thermal hysteresis, the intensity of the random coil peak is not recovered even upon cooling well below the T_{cp} (Fig. 2, C and D). Moreover, for short and long IDPPs of the hexapeptide TPVAVG, all of which show very large hysteresis (fig. S2A), the initial decrease in the intensity of the random coil peak at the T_{cp} on heating is followed by the emergence of an unusually broad negative peak at ~210 nm (Fig. 2, B and C) at the plateau region of the turbidity profile. IDPPs composed of VAPVG repeats also showed this type of CD spectrum upon their LCST phase transition and throughout the hysteretic region (Fig 2B) but only for polymers above a threshold number of pentapeptide repeats (~40) that is required to encode robust hysteretic phase behavior (Fig. 2, A and B). This similarity in hysteresis-associated CD spectra between IDPPs that exhibit widely different degrees of thermal hysteresis indicates that additional sequence-encoded features, besides those that dictate backbone rigidity (i.e., secondary structure dynamics as probed by CD), must govern the extent of this behavior.

By analogy to the observation that related proteins with high sequence and structural similarity [e.g., superfolder green fluorescent protein (GFP) and enhanced GFP] may exhibit distinct chemical and thermal stabilities (*28*), we next investigated the phase behavior of hysteretic IDPPs in the presence of urea, a potent chaotrope that is frequently used as a protein denaturant. First, increasing amounts of urea readily shifted the T_{cp} on heating to higher temperatures, and the extent of this effect was identical for IDPPs with negligible, moderate, or large hysteresis and was independent of repeat number (Fig. 3A and fig. S5). Urea similarly increased the T_{cp} of canonical ELPs (fig. S5D) (*29*), which suggests that irrespective of their hysteretic behavior, LCST IDPPs undergo a canonical phase transition driven by desolvation of the polymer chain upon heating. Upon cooling, urea decreased the degree of thermal hysteresis in IDPPs with moderate hysteretic behavior (Fig. 3B). For example, at 1 M urea, we observed a 75% reduction in the degree of thermal hysteresis of $(VAPVG)_{80}$ (Fig. 3B). Increasing the concentration of denaturant for IDPPs with moderate hysteresis resulted in a corresponding decrease in hysteresis (Fig. 3B).

Polymers that exhibit large, environmentally sensitive hysteresis, such as polymers of VGPVG and TPVAVG repeats (Fig. 3C and fig. S5, B, C, E, and F), showed no reduction in hysteresis up to 4 M urea. Because these two IDPPs display environmentally sensitive hysteresis, we repeated these experiments without exceeding their critical threshold temperature (~45°C). Under these conditions, high concentrations of urea decreased thermal hysteresis of $(TPVAVG)_{80}$ (Fig. 3D). However, unlike the rapid decline in hysteresis that urea triggered for $(VAPVG)_{80}$, $(TPVAVG)_{80}$ still showed sizable hysteresis (~31°C) in 2 M urea (Fig. 3D), and the percent reduction from 1 to 2 M urea was only 30%—in contrast to 60% for $(VAPVG)_{80}$. While we cannot pinpoint yet the molecular origins of the critical threshold temperature below which IDPPs with otherwise large hysteresis phase transition without hysteresis, our recent molecular dynamics (MD) studies of a canonical, nonhysteretic ELP—$(VPGVG)_{18}$—in explicit water revealed a critical temperature window (~55° to 60°C in that polymer-water system) at which peptide hydration is drastically reduced, concomitant with a pronounced increase in the strength of peptide-peptide interactions (*30*). This molecular insight suggests that the rehydration dynamics of hysteretic IDPPs may be hampered if heated above a critical temperature window defined by temperature-dependent peptide-water interactions.

The intersection of our CD data and urea denaturation studies point to the molecular origins of the unique and robust hysteretic phase behavior of LCST IDPPs. We surmise that the emergence of order in the polymer-rich phase stabilizes the aggregated phase by increasing molecular rigidity (*31*)—hence reducing chain mobility—and by facilitating the formation of metastable interchain interactions that are not easily disrupted by cooling or protein denaturants. This view also rationalizes the rapid and progressive loss of reversibility that we observed in UCST IDPPs (fig. S3, A and B), as they are generally enriched in amino acids capable of extensive hydrogen bonding. Analogous to LCST IDPPs, however, this nonequilibrium behavior is readily countered by urea (fig. S3C) and by mutations at the repeat level that reduce polymer rigidity (fig. S3D). Because these stabilizing interactions can limit the dynamic and liquid-like nature of phase-separated polymers (*32*), we imaged the coalescence process of fluorescently labeled $(VPAVG)_{40}$, a polymer with moderate hysteresis

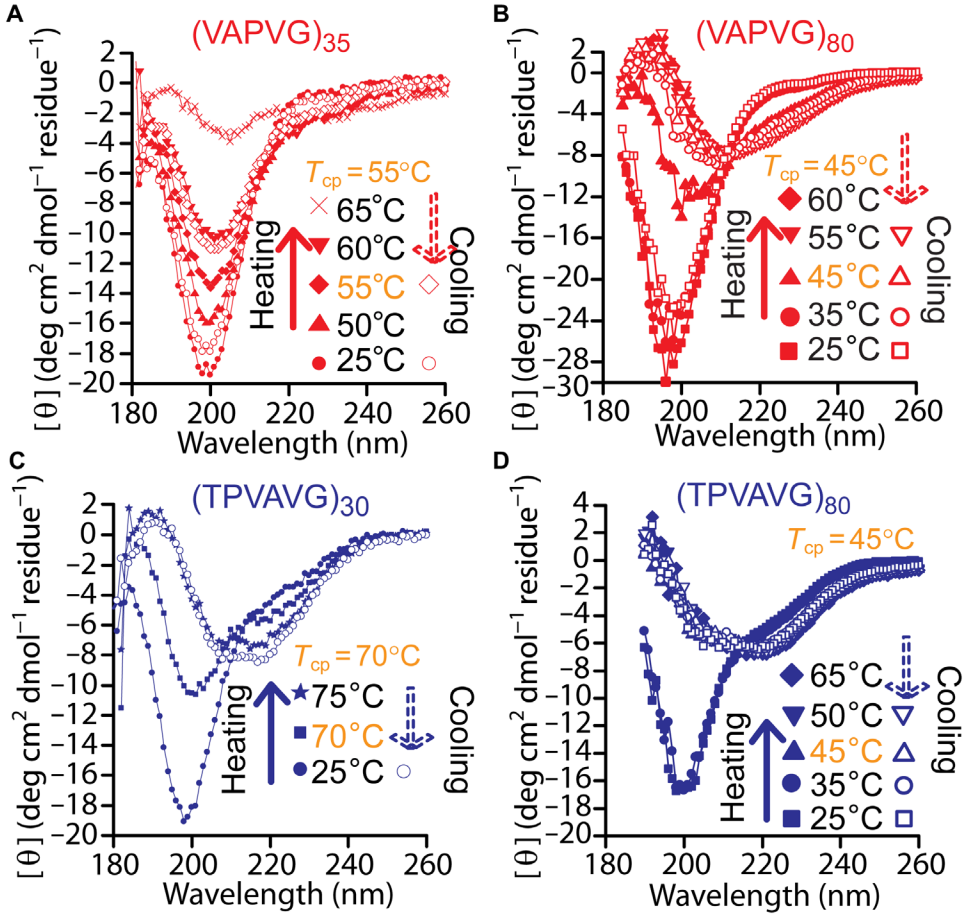

Fig. 2. Hysteretic LCST IDPPs within the marked hysteretic regime exhibit structural dynamics that deviate from the behavior of canonical IDPs. (**A** and **B**) CD data as a function of temperature for two IDPPs, consisting of either 35 (A) or 80 (B) (VAPVG) repeats and displaying ~5°C wide (A) or ~15°C wide (B) thermal hysteresis in their phase behavior when triggered at an IDPP concentration of 5 μM in water. (**C** and **D**) CD data as a function of temperature for two IDPPs, consisting of either 30 (C) or 80 (D) (TPVAVG) repeats. Solutions of both IDPPs at a concentration of 5 μM in water display large degrees of thermal hysteresis (>50°C) in their phase behavior. For all IDPPs shown here, the T_{cp} was calculated from optical turbidity data obtained under the same experimental conditions (5 μM in water) as our CD spectroscopy data. For simplicity, mean residue ellipticity (θ) values are shown as $\theta*10^{-3}$.

during its coacervation, and observed the formation of an arrested network that differed from the spherical droplets formed by the coalescence of highly dynamic nonhysteretic IDPPs as they undergo their LCST phase transition (fig. S6). In line with these observations, among synthetic polymers, we note the slight degree of thermal hysteresis (~3°C) seen for polymers of *N*-isopropylmethacrylamide—attributed to increased polymer-polymer hydrogen bonding and reduced flexibility (*33*)—and the moderate thermal hysteresis (~20°C) seen in the LCST behavior of polysaccharides such as methylcellulose (*14*), as only the latter assume rather rigid conformations and engage in substantial hydrogen bonding (*34*).

Subtle changes in amino acid syntax drastically alter hysteresis

To further examine the role of peptide-peptide interactions that ought to be sensitive to amino acid order, instead of simply depending on compositional effects, we considered pairs of motifs in our library that are related to each other by sequence reversal. This strategy was appealing to us because the resulting "retro" sequence is identical to the parent sequence if the concatenated repeats are read from C to N terminus, so that the overall composition and other physicochemical properties remain unaltered (Fig. 4A). In addition, because our motifs are low complexity sequences, their syntax—read from N to C terminus—differs only slightly at specific dipeptides (e.g., PG/GP and PA/AP) or tripeptides (e.g., VPA/AVP) within the repeat. We synthesized and characterized four different IDPP pairs, wherein each polymer in a pair corresponds to the forward or reverse sequence. All of these IDPPs shared similar CD spectra, characteristic of IDPs, below their T_{cp} (fig. S7). Examination of their phase behavior on heating suggested minor or negligible changes in their T_{cp} (Fig. 4, B to D). However, upon cooling below the T_{cp} on heating, we observed marked changes in the LCST behavior of three of these pairs, namely, pronounced differences in the degree of thermal hysteresis between members of each pair (Fig. 4, B to D). The phase behavior of only one of these pairs was not affected by sequence reversal (Fig. 4C). These marked changes in thermal hysteresis due to subtle changes in syntax of the repeat unit suggest a major role for syntax in governing the phase behavior of LCST IDPPs.

From an engineering perspective, the exquisite sensitivity to syntax demonstrated here sets LCST IDPPs far apart from synthetic polymers that exhibit LCST behavior in aqueous solutions. While the LCST phase behavior of synthetic random copolymers can be tuned by

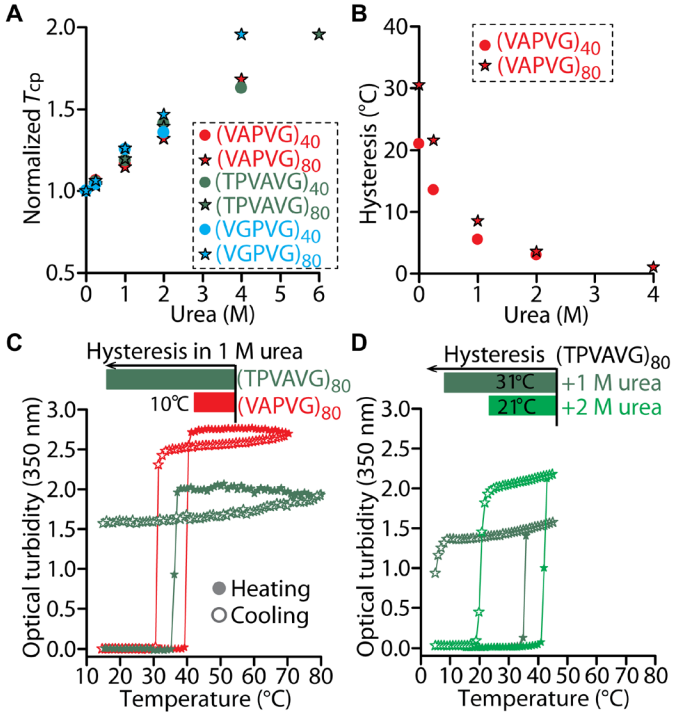

Fig. 3. A protein denaturant modulates the hysteretic phase behavior of LCST IDPPs. (**A**) Cloud point temperatures as a function of increasing concentrations of a protein denaturant (urea) in PBS for IDPPs with negligible—$(VPGVG)_{40}$ and $(VPGVG)_{80}$; see fig. S5—moderate—$(VAPVG)_{40}$ and $(VAPVG)_{80}$—and large—$(TPVAVG)_{40}$, $(TPVAVG)_{80}$, $(VGPVG)_{40}$, and $(VGPVG)_{80}$—hysteresis. Values were normalized to T_{cp} in PBS without urea. To overcome the overlapping of normalized T_{cp}'s, these data are also presented as separate panels in fig. S5. (**B**) Degree of thermal hysteresis for IDPPs made of VAPVG repeats at a fixed concentration of 50 μM in PBS supplemented with increasing amounts of urea. (**C**) Temperature-dependent optical turbidity data in PBS + 1 M urea for two IDPPs with identical repeat number but different repeat motifs that encode widely different hysteretic behaviors. Even in 4 M urea, 40-mer IDPPs of TPVAVG repeats display pronounced hysteretic behavior (fig. S5). (**D**) Phase behavior data as in (C), in PBS with 1 or 2 M urea, but exclusively for $(TPVAVG)_{80}$ and when the phase transition is triggered without exceeding 45°C during the heating cycle. All relevant T_{cp} values were calculated from optical turbidity data at a concentration of 50 μM in PBS or PBS supplemented with urea as indicated.

their composition, as seen by the systematic change in their T_{cp} as a function of monomer composition, other features of their phase behavior such as thermal hysteresis cannot yet be tuned because of the inability to control their syntax. In contrast, the precise control of syntax and chain length allows LCST IDPPs to be synthesized with a wide range of thermal hysteresis. These results also underscore the fact that the inability of synthetic polymers to access previously unknown LCST properties via sequence control is one example of the grand challenge of sequence control in polymer chemistry (*35*).

Native IDPs with distinct assembly behaviors diverge at the syntax level

The observation that syntax can affect thermal hysteresis prompted us to next examine whether subtle differences in the syntax of Pro- and Gly-rich IDPs might control their binary propensity to exhibit elastomeric versus amyloidogenic behavior (*36*). While the overall Pro and Gly content is a known factor that controls the behavior of IDPs (*36*), the phase behavior of sequence-reversed IDPPs shows that syntax has a bearing on their properties as well. Specifically, we were surprised by the marked differences in phase behavior between an IDPP of the prototypical ELP motif, VPGVG, and an IDPP of its sequence-reversed motif, GVGPV (Fig. 4B), as these two IDPPs only differ in whether they repeat a PG or a GP dipeptide—all other residues arrange in the same sequence as the repeat units concatenate in the IDPP.

Because Pro- and Gly-rich IDPs in nature could arrange Pro and Gly along their sequence to either favor or prevent the occurrence of PG or GP dipeptides, we asked whether known differences in their properties may be explained, at least partly, by this subtle change in syntax. We recently reported that the sequence of Pro- and Gly-rich IDPs (Fig. 4F) is populated by abundant PG dipeptides that recur as part of a larger family of P-X_n-G motifs (where X is any residue except P/G and n = 0 to 4) (*10*). To consider all possible PG- and GP-containing sequences in these proteins, we examined the occurrence of Gly in residue positions (Z_i) surrounding P-X_n-G motifs (Z_{-2}-Z_{-1}-P-X_n-G-Z_{+1}-Z_{+2} motifs, where Z_i is any residue; see Supplementary Methods). This analysis revealed a highly biased localization of Gly residues that differed between IDPs that usually form amorphous aggregates such as elastin, resilin, and gluten and IDPs that tend to form fibrillar structures such as collagen and silks. We found that Gly is nonrandomly and consistently ($P < 0.001$, see Supplementary Methods) absent one residue N-terminal (Z_{-1}) to P-X_n-G motifs in the coacervating group of proteins, whereas it is enriched, leading to abundant GP dipeptides, at that position in the fibril-forming group (Fig. 4G). This suggests a potential role for Gly at this position in controlling whether Pro- and Gly-rich IDPs go down the (reversible) coacervation or the (irreversible) fibril-forming amyloidogenic pathway. Motifs in our library that prevent the formation of GP dipeptides by substituting Gly at this position by bulkier residues consistently led to elimination or reduction of their thermal hysteresis (Fig. 4H and fig. S8). While this may explain the evolutionary pressure against Gly at this position in nonfibrillar, Pro- and Gly-rich IDPs, because other factors are also likely to be at play, more in-depth studies will be required to dissect these conspicuous sequence biases in IDPs.

MD reveal peptide-peptide interactions at the crux of hysteresis

To further examine the intriguing role of syntax in the hysteretic phase behavior of LCST IDPPs, we turned to all-atom MD simulations. While the study of phase behavior in proteins through simulation remains a major challenge due to the cooperative nature of this process, we recently reported an MD approach to study peptide-peptide and peptide-water interactions of a canonical ELP, $(VPGVG)_{18}$, and $(VGPVG)_{18}$ in explicit water and over a wide temperature range (*30*, *37*). Here, we exploit this MD approach to examine, at the molecular level, the behavior of syntactically related IDPP pairs that exhibit either markedly different degrees of thermal hysteresis (motif pairs in Fig. 4, B and C) or nearly identical behaviors with negligible hysteresis (motif pair in Fig. 4D).

At the single-molecule level, sequence reversal resulted in minor changes in secondary structure propensities (Fig. 5A and fig. S9, A to C), with all IDPPs predominantly sampling unstructured motifs at high and low temperatures irrespective of their type of hysteretic phase behavior (Fig. 5A). These MD data agree with our CD data on these IDPPs below their T_{cp}, which consistently showed spectra characteristic of disordered proteins (fig. S7). As discussed in our

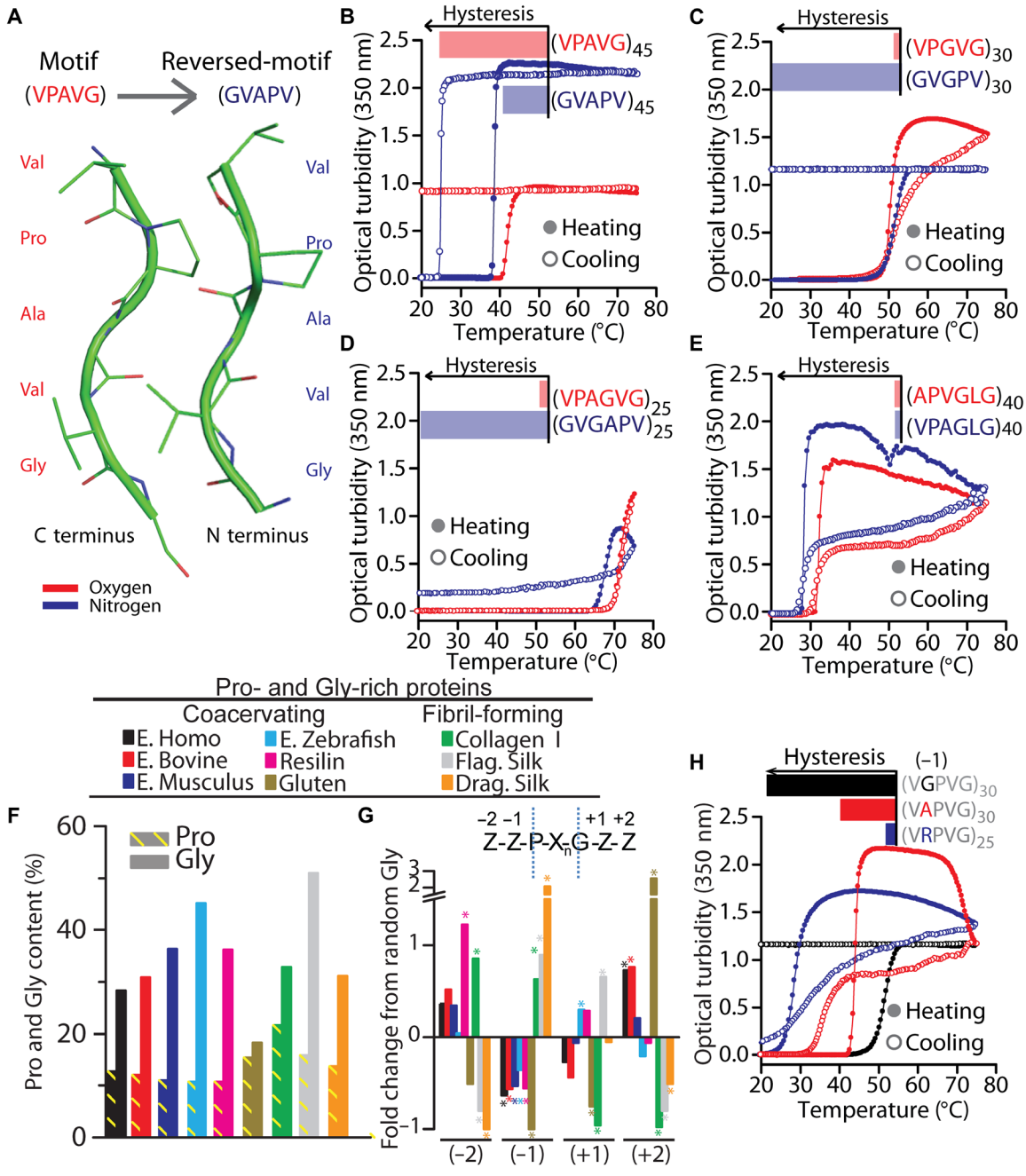

Fig. 4. Subtle changes in repeat syntax can have profound effects on the hysteretic phase behavior of IDPPs and their related native IDPs. (**A**) Peptide motifs that relate to each other by simple sequence reversal—rewriting a peptide sequence by reading it from C to N terminus—present identical patterns of amino acid side chains, which we illustrate with the structure of a pentapeptide motif and its reversed motif as observed in the crystal structures of two different proteins (Protein Data Bank ID 3MKR_B and 1OZP, respectively). The images were rendered using PyMOL (http://pymol.org/). (**B** to **E**) Temperature-dependent optical turbidity to probe the phase behavior of four IDPP pairs, wherein each pair consists of two IDPPs with identical number of repeats of motif sequences that are interrelated by sequence reversal. As a guide to the eye, each panel includes a legend with a qualitative indicator of the degree of hysteresis for each IDPP. Figure S7 shows CD spectroscopy at 25°C that reaffirms the intrinsic disorder of these IDPP pairs before their phase transition. (**F**) Pro and Gly content of a representative group of Pro- and Gly-rich IDPs that we previously characterized as being enriched in Pro-X_n-Gly motifs (*10*). (**G**) Enrichment or depletion of Gly in residue positions surrounding P-X_n-G motifs among Pro- and Gly-rich IDPs, expressed as a fold change from the random occurrence of Gly based on total Gly content. Asterisks indicate significant ($P < 0.001$) divergence from a random distribution (see Supplementary Methods). (**H**) Temperature-dependent turbidimetry of an IDPP composed of a motif wherein Gly occurs one residue N-terminal to P-X_n-G and corresponding mutant polymers wherein Gly was substituted by bulkier amino acids. All turbidity measurements were conducted in PBS at an IDPP concentration of 50 μM, except for VRPVG (+1 M NaCl).

previous study, the average radius of gyration (R_g) of a single $(VPGVG)_{18}$ chain gradually declines as temperature increases (*30*). Here, we observed the same phenomenon, reflected by negative values for the R_g differential between simulations at high and low temperatures, but only for the members of each IDPP pair that exhibited negligible hysteresis in our experiments: $(VPAGVG)_{18}$, $(VPAGLG)_{18}$, and $(LGAPVG)_{18}$ (Fig. 5B). In contrast, whenever sequence reversal led to large hysteresis experimentally, as in (VGPVG) (Fig. 4C) and (VGAPVG) (Fig. 4D), the R_g differential was close to zero, as it stayed approximately the same at high and low temperatures, indicating increased backbone rigidity and a less compact conformation compared with nonhysteretic polymers. We also measured temperature-related changes in peptide-water interaction energy (E_{pw}) to examine the role of hydrophobic hydration in hysteresis. Figure 5B shows absolute values for changes in E_{pw}, which are naturally negative because the interaction between proteins and water becomes energetically unfavorable as temperature increases. Contrary to a major role for hydrophobic hydration in hysteresis, hysteretic IDPPs, $(VGPVG)_{18}$, and $(VGAPVG)_{18}$ showed markedly smaller (absolute) changes in E_{pw} compared with their reversed, nonhysteretic motifs or even the control IDPP pair in which both members are nonhysteretic (Fig. 5B). The relatively small difference in E_{pw} indicates that the surface hydrophobicity of these two hysteretic IDPPs did not change significantly over a temperature range wherein nonhysteretic IDPPs already experience substantial changes in hydration and chain collapse (e.g., decreasing R_g). These insights suggest that even at temperatures above their T_{cp}, hysteretic IDPPs may remain extended and expose residues that engage in interchain interactions (e.g., hydrogen bonding) that stabilize the aggregated phase.

To gain understanding of the molecular forces that sustain hysteresis during cooling, we first performed long MD simulations at high temperatures (350 to 370 K) of two closely interacting IDPP chains using a periodic box with explicit water. The end point of

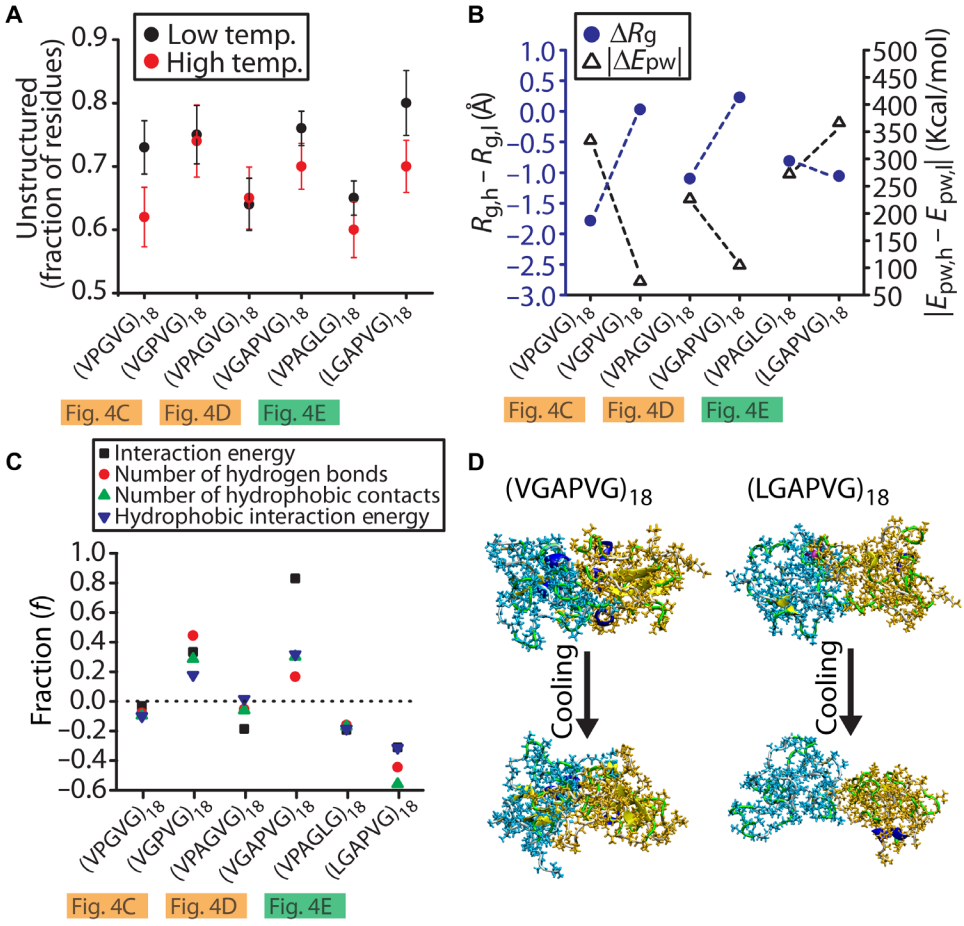

Fig. 5. MD simulations of syntactically related IDPPs reveal interchain interaction forces that promote hysteresis. (**A** and **B**) Simulations of 18-mer, single IDPP chains at low (290 to 310 K) and high (350 to 390 K) temperatures for three IDPP pairs studied in Fig. 4 (C to E). (A) Fraction of residues that are part of unstructured motifs for single IDPP chains at high and low temperatures (see fig. S9 for all other structural motifs). (B) Temperature-dependent changes in radius of gyrations (R_g, black) and absolute peptide-water interaction energy (E_{pw}, blue), expressed as a differential between values at high and low temperatures (ΔR_g and ΔE_{pw}). Dashed lines between data points for IDPPs in each pair are guides to the eye. (**C** and **D**) Simulations of two closely interacting 18-mer IDPP chains for each IDPP in Fig. 4 (C to E) to study interchain interactions in a model phase separated state. (C) Fraction of value changes (f) in interchain interaction quantities (see Supplementary Methods for details) after cooling these two chain "phase separated" systems to 290 K for 25 ns. f = (end value − initial value)/(initial value). (D) Snapshots from our two-chain simulations for an IDPP with marked hysteresis $(VGAPVG)_{18}$ (Fig. 4D) and for an IDPP with negligible hysteresis $(LGAPVG)_{18}$ (Fig. 4E). The production simulations were performed for 25 ns with a 2-fs time step.

these simulations served as a model of two chains aggregating and provided the starting conditions for a subsequent "quenching" (cooling) process to 290 K. We calculated several interaction parameters between the two IDPP chains before and after cooling: interaction energy, number of interchain hydrogen bonds, number of interchain hydrophobic contacts, and (absolute) hydrophobic interaction energy. Figure 5C shows the fractional change in these interchain interaction parameters. Fraction (*f*) is set to be (Pe – Pb)/Pb, where Pe is the parameter value after cooling the aggregates (at 25 ns of simulation time), and Pb is the parameter value at high temperature before cooling. This two-chain model of IDPP aggregation effectively pointed to large differences in interpeptide interaction forces as a major driver of hysteresis, as only those IDPPs within each pair that exhibited hysteretic phase behavior showed a positive fractional difference in all measured interchain parameters, whereas all IDPPs that lacked hysteresis—including $(APVGLG)_{18}$ and its sequence reversed counterpart $(GLGVPA)_{18}$—consistently showed negative fractions (Fig. 5D). These differences in interaction energy are discernible from snapshots at the end of our cooling simulations, in which the two chains of a hysteretic IDPP continue to closely interact, whereas the two chains of a nonhysteretic IDPP lose contact with each other (Fig. 5D). While qualitative in nature, the sustained interactions that become apparent in this two-chain aggregate model likely reflect the quantitative differences that distinguish between hysteretic and nonhysteretic IDPs, namely, their backbone rigidity and extended conformations (Fig. 5B) that favor interchain interactions through increased hydrogen bonding and hydrophobic contacts (Fig. 5C). Overall, these data suggest that IDPPs with large hysteresis are unique among LCST IDPPs in their ability to form intermolecular interactions, namely, hydrogen bonds and hydrophobic contacts, and to sustain these interactions during cooling—at least in the initial stages—to temperatures that readily disaggregate nonhysteretic IDPPs that favor equilibrium phase behavior.

IDPPs with hysteretic phase behavior offer new tools to control protein assemblies

We reasoned that the tunable thermal hysteresis of LCST IDPPs offered a previously unidentified design variable to control block-copolymer assembly (Fig. 6A). To explore this possibility, we studied two diblock copolymers composed of the same corona-forming block—an ELP with

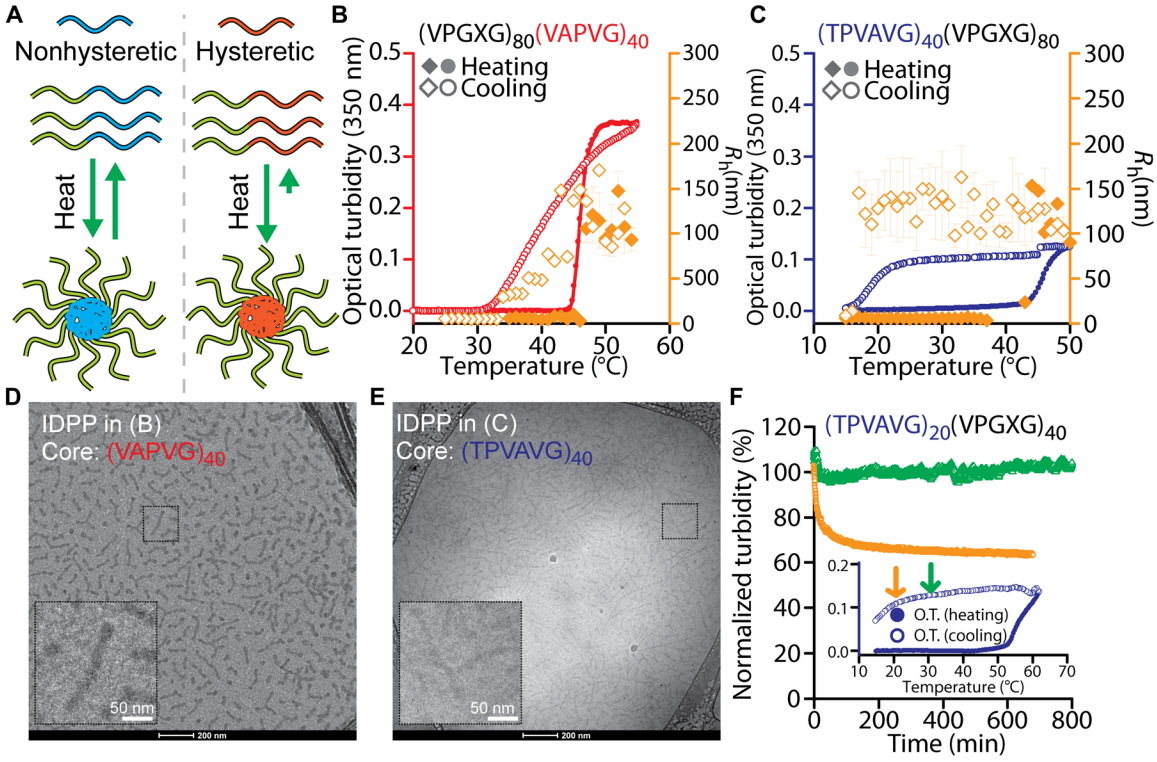

Fig. 6. Hysteretic LCST phase behavior enables the synthesis of morphologically diverse nanoparticles that resist disassembly. (**A**) The nonequilibrium phase behavior of hysteretic LCST IDPPs may affect the thermally triggered assembly of protein-based block copolymers into micelles. (**B** and **C**) By synthesizing diblock copolymers composed of a common hydrophilic, corona-forming ELP block $(VPGXG)_{80}$, where X = [A:G], and hydrophobic, core-forming blocks that repeat a hysteretic LCST motif with either (B) moderate (VAPVG) or (C) large (TPVAVG) hysteresis, we synthesized self-assembling nanoparticles that remain assembled below the critical assembly temperature in proportion to the degree of thermal hysteresis of the core-forming block. Their temperature-dependent assembly was studied using UV-visible spectroscopy, shown as small changes in optical turbidity (<0.4 U at 350 nm, circles), and by dynamic light scattering that revealed large changes in hydrodynamic radius (R_h, diamonds). Heating and cooling were performed at 1°C/min. Error bars are the measured polydispersity. (**D** and **E**) Cryo-TEM images show that diblock IDPPs with similar block architecture and hydropathy balance assemble into distinct rod-like morphologies by virtue of the unique hysteretic phase behavior of the core-forming blocks. Scale bars in large fields of view are 200 nm. Scale bars within insets are 50 nm. (**F**) Time-dependent stability of nanoparticles formed by a diblock copolymer with the same repeat composition and block ratio as in (C) and (E) but having half the number of repeats in the (TPVAVG) core. Stability was studied as normalized optical turbidity (normalized to time zero) as a function of time at two constant temperatures (arrows) that are well below the critical assembly temperature—inset shows temperature-dependent changes in optical turbidity (O.T.).

a T_{cp} of 60°C—and different hydrophobic, core-forming blocks consisting of IDPPs with distinct hysteretic phase behaviors but T_{cp} values that only differed by 4°C. Dynamic light scattering as a function of temperature shows that these diblock IDPPs form nanoparticles (Fig. 6, B and C) of unusually large hydrodynamic radius (R_h) compared with typical ELP micelles (~20 to 30 nm) that self-assemble from ELP copolymers of similar length (*38*), suggesting that these hysteretic IDPPs do not form the spherical micelles that typically form by temperature-triggered self-assembly of diblock copolymers of canonical ELPs (*39*). Moreover, large differences in their optical turbidity at 350 nm (Fig. 6, B and C) suggested that each diblock assembled into a different nanostructure. We then turned to Cryo-TEM, which demonstrated the distinct rod-like morphology of these nanoparticles (Fig. 6, D and E). This morphological diversity is intriguing, as nanoparticle morphology is a well-known modulator of tissue distribution and pharmacokinetics (*40*).

The degree of thermal hysteresis in the core-forming block also directly controlled nanoparticle stability on cooling below the critical assembly temperature (Fig. 6, B to D). Figure 6B shows that the moderate hysteresis of a core-forming IDPP partially stabilized the nanoparticles below the critical assembly temperature but only for a temperature range that is consistent with its degree of thermal hysteresis (~10°C). In contrast, when the core-forming block corresponded to an IDPP with large hysteresis, this behavior prevented the disassembly of the nanoparticles on cooling over a broad temperature range below the critical assembly temperature, as seen by consistent optical turbidity and R_h values in the large hysteretic region (Fig. 6C). The role of repeat number in determining the hysteretic phase behavior of core-forming IDPPs and hence the stability of the resulting nanoparticles was explored by synthesizing a related but shorter diblock copolymer that kept the core to corona block ratio constant. Despite the relatively small size of this core-forming block, $(TPVAVG)_{20}$, self-assembly was sustained through a broad hysteretic region, and these nanoparticles remained stable for at least 13 hours at temperatures near the end of the hysteretic range (Fig. 6D), which agrees with the strong hysteretic behavior displayed by $(TPVAVG)_{20}$ (fig. S2A). Besides the well-known roles of amphiphilicity and block architecture (i.e., relative size and order of blocks) in dictating self-assembly of protein polymers (*39*, *41*), our findings point to the rich set of phase behaviors that can be encoded at the repeat level as a useful variable to manipulate the equilibrium properties of these self-assemblies.

Outlook

This work demonstrated that IDPPs can access a wide range of hysteretic phase separation behaviors that offer a route to encode non-equilibrium properties in self-assembling materials. Because we show that hysteresis can be genetically encoded with molecular precision, at the repeat level and at the macromolecule level, these findings may inform the phase separation behavior of poorly understood IDPs in nature and enable a systematic exploration of sequence space to uncover novel material properties in protein-based materials. Last, the peptide-peptide interaction forces that drive hysteretic phase behavior in IDPs constitute a previously unknown variable—distinct from block architecture/amphiphilicity—to control the bottom-up assembly of stimuli-responsive material systems that is likely to yield diverse nanostructured materials with tunable stability for applications in medicine and biotechnology.

MATERIALS AND METHODS

Genetically encoded synthesis of IDPPs

We relied on our recently published library (*10*) of genes encoding IDPPs that exhibit LCST or UCST phase behavior, which we generated using overlap extension rolling circle amplification (*42*). To further study hysteretic phase behavior of specific IDPPs, with full control on repeat number, we generated additional IDPP-coding genes using recursive directional ligation by plasmid reconstruction (Pre-RDL) (table S1) (*43*). For the synthesis of genes encoding diblock IDPPs, we used Pre-RDL for the genetic fusion of full-length IDPP genes with a previously reported ELP gene encoding VPGXG repeats (X = [A:G]) of varying length (*43*).

IDPP expression and purification

IDPPs were produced in *Escherichia coli* BL21(DE3) from plasmid-borne genes after overnight induction with 1 mM isopropyl-β-D-thiogalactopyranoside. LCST polymers were purified by inverse transition cycling (see Supplementary Methods for details). UCST IDPPs were purified as previously reported (*10*).

Characterization of the phase transition behavior and secondary structure of IDPPs

The phase behavior of LCST and UCST IDPPs was characterized by temperature-dependent measurements of their optical turbidity at 350 nm (at the concentrations indicated in figures but typically at 50 μM) in PBS, with heating and cooling performed at a rate of 1°C/min except when indicated in the text or figures, on a Cary 300 ultraviolet (UV)–visible spectrophotometer equipped with a multicell thermoelectric temperature controller. The temperature-dependent changes in secondary structure exhibited by IDPPs were studied by CD spectroscopy, using an Aviv Model 202 instrument and 1-mm quartz cells, at a fixed concentration of 5 μM in water.

Quantitative analysis of Gly residues surrounding P-X_n-G motifs

Using a custom-made script (Script 1 in Supplementary Methods; MATLAB R2013a), we quantified the abundance of Gly in residue positions surrounding P-X_n-G motifs in a previously reported set of Pro and Gly-rich IDPs (*10*). Briefly, we estimated "fold change from random Gly" (FCRG), calculated according to eq. S1 (Supplementary Methods). Positive values of FCRG indicate an enrichment of Gly, whereas negative values suggest a depletion of Gly with respect to the probability of occurrence of Gly expected from the overall Gly content of each protein. We considered that a given FCRG value was statistically significant when its *P* value was equal or lower than 0.001 (see Supplementary Methods for details).

Molecular dynamics

Fully atomistic MD simulations were performed using Amber 12.07 and the ff99SB force field for proteins with explicit solvent using the TIP3P water model. Extensive descriptions of our simulation strategy for single- and two-chain simulations are presented in our previous research papers (*30*, *37*), and all relevant details of simulations in this study are included in the Supplementary Methods.

Nanoparticle characterization

Temperature-dependent self-assembly of diblock IDPPs was studied at a fixed concentration of 50 μM in PBS, by optical turbidity measurements on a UV-visible spectrophotometer (Cary 300) and dynamic

light scattering measurements on a Wyatt DynaPro temperature-controlled microsampler. Heating and cooling were performed at ~1°C/min. We also conducted Cryo-TEM at Duke University's Shared Materials Instrumentation Facility (Durham, NC) using Lacey holey carbon grids (Ted Pella, Redding, CA) and a Vitrobot Mark IV (FEI, Eindhoven, The Netherlands) for blotting and vitrification. We triggered nanoparticle assembly by incubating samples (50 μM in PBS) at 50°C for 15 min. We then loaded samples onto grids within the vitrification chamber set to either 50°C (Fig. 6D) or 30°C (Fig. 6E) and at 100% relative humidity. After vitrification, grids were transferred to a Gatan 626 cryoholder (Gatan, Pleasanton, CA) and imaged on a FEI Tecnai G2 Twin TEM (FEI, Eindhoven, The Netherlands), operating under low-voltage conditions at 80 keV.

SUPPLEMENTARY MATERIALS

Supplementary material for this article is available at http://advances.sciencemag.org/cgi/content/full/5/10/eaax5177/DC1

Supplementary Methods

Table S1. DNA sequence information for synthesis of genes encoding IDPPs by Pre-RDL.

Fig. S1. LCST IDPPs display large, environmentally sensitive hysteresis.

Fig. S2. Repeat number influences the hysteretic phase behavior of LCST IDPPs.

Fig. S3. Forms of irreversible phase behavior in UCST IDPPs.

Fig. S4. LCST IDPPs exhibit CD spectra characteristic of intrinsic disorder and regardless of their hysteretic nature.

Fig. S5. Effect of urea on the hysteretic phase behavior of IDPPs.

Fig. S6. Imaging of nonhysteretic and hysteretic IDPPs upon phase separation.

Fig. S7. Secondary structure of IDPPs related by sequence reversal at the repeat level.

Fig. S8. Steric hindrance at the residue position preceding a P-Xn-G motif influences hysteresis.

Fig. S9. Secondary structure preferences calculated from single-chain IDPP simulations at low and high temperatures.

References (*44*–*53*)

View/request a protocol for this paper from *Bio-protocol*.

REFERENCES AND NOTES

1. M. A. C. Stuart, W. T. S. Huck, J. Genzer, M. Müller, C. Ober, M. Stamm, G. B. Sukhorukov, I. Szleifer, V. V. Tsukruk, M. Urban, F. Winnik, S. Zauscher, I. Luzinov, S. Minko, Emerging applications of stimuli-responsive polymer materials. *Nat. Mater.* **9**, 101–113 (2010).
2. J. R. McDaniel, D. J. Callahan, A. Chilkoti, Drug delivery to solid tumors by elastin-like polypeptides. *Adv. Drug Deliv. Rev.* **62**, 1456–1467 (2010).
3. K. Nishida, M. Yamato, Y. Hayashida, K. Watanabe, K. Yamamoto, E. Adachi, S. Nagai, A. Kikuchi, N. Maeda, H. Watanabe, T. Okano, Y. Tano, Corneal reconstruction with tissue-engineered cell sheets composed of autologous oral mucosal epithelium. *N. Engl. J. Med.* **351**, 1187–1196 (2004).
4. P. Koria, H. Yagi, Y. Kitagawa, Z. Megeed, Y. Nahmias, R. Sheridan, M. L. Yarmush, Self-assembling elastin-like peptides growth factor chimeric nanoparticles for the treatment of chronic wounds. *Proc. Natl. Acad. Sci. U.S.A.* **108**, 1034–1039 (2011).
5. S. Roberts, T. S. Harmon, J. L. Schaal, V. Miao, K. Li, A. Hunt, Y. Wen, T. G. Oas, J. H. Collier, R. V. Pappu, A. Chilkoti, Injectable tissue integrating networks from recombinant polypeptides with tunable order. *Nat. Mater.* **17**, 1154–1163 (2018).
6. D. E. Meyer, A. Chilkoti, Purification of recombinant proteins by fusion with thermally-responsive polypeptides. *Nat. Biotechnol.* **17**, 1112–1115 (1999).
7. P. S. Stayton, T. Shimoboji, C. Long, A. Chilkoti, G. Ghen, J. M. Harris, A. S. Hoffman, Control of protein–ligand recognition using a stimuli-responsive polymer. *Nature* **378**, 472–474 (1995).
8. S. F. Banani, H. O. Lee, A. A. Hyman, M. K. Rosen, Biomolecular condensates: organizers of cellular biochemistry. *Nat. Rev. Mol. Cell Biol.* **18**, 285–298 (2017).
9. S. Alberti, A. Gladfelter, T. Mittag, Considerations and challenges in studying liquid-liquid phase separation and biomolecular condensates. *Cell* **176**, 419–434 (2019).
10. F. G. Quiroz, A. Chilkoti, Sequence heuristics to encode phase behaviour in intrinsically disordered protein polymers. *Nat. Mater.* **14**, 1164–1171 (2015).
11. J. Wang, J.-M. Choi, A. S. Holehouse, H. O. Lee, X. Zhang, M. Jahnel, S. Maharana, R. Lemaitre, A. Pozniakovsky, D. Drechsel, I. Poser, R. V. Pappu, S. Alberti, A. A. Hyman, A molecular grammar governing the driving forces for phase separation of prion-like RNA binding proteins. *Cell* **174**, 688–699. e16 (2018).
12. F. Käfer, F. Liu, U. Stahlschmidt, V. Jérôme, R. Freitag, M. Karg, S. Agarwal, LCST and UCST in One: Double Thermoresponsive Behavior of Block Copolymers of Poly(ethylene glycol) and Poly(acrylamide-*co*-acrylonitrile). *Langmuir* **31**, 8940–8946 (2015).
13. C. M. Elvin, A. G. Carr, M. G. Huson, J. M. Maxwell, R. D. Pearson, T. Vuocolo, N. E. Liyou, D. C. C. Wong, D. J. Merritt, N. E. Dixon, Synthesis and properties of crosslinked recombinant pro-resilin. *Nature* **437**, 999–1002 (2005).
14. S. Fujishige, K. Kubota, I. Ando, Phase transition of aqueous solutions of poly (N-isopropylacrylamide) and poly (N-isopropylmethacrylamide). *J. Phys. Chem.* **93**, 3311–3313 (1989).
15. J. Reguera, J. M. Lagarón, M. Alonso, V. Reboto, B. Calvo, J. C. Rodríguez-Cabello, Thermal behavior and kinetic analysis of the chain unfolding and refolding and of the concomitant nonpolar solvation and desolvation of two elastin-like polymers. *Macromolecules* **36**, 8470–8476 (2003).
16. J. Seuring, S. Agarwal, Polymers with upper critical solution temperature in aqueous solution. *Macromol. Rapid Commun.* **33**, 1898–1920 (2012).
17. F. Käfer, A. Lerch, S. Agarwal, Tunable, concentration-independent, sharp, hysteresis-free UCST phase transition from poly (*N*-acryloyl glycinamide-acrylonitrile) system. *J. Polym. Sci. A Polym. Chem.* **55**, 274–279 (2017).
18. S. Kuroyanagi, N. Shimada, S. Fujii, T. Furuta, A. Harada, K. Sakurai, A. Maruyama, Highly Ordered Polypeptide with UCST phase separation behavior. *J. Am. Chem. Soc.* **141**, 1261–1268 (2019).
19. A. Halperin, M. Kröger, F. M. Winnik, Poly (*N*-isopropylacrylamide) phase diagrams: Fifty years of research. *Angew. Chem. Int. Ed.* **54**, 15342–15367 (2015).
20. D. Mozhdehi, K. M. Luginbuhl, J. R. Simon, M. Dzuricky, R. Berger, H. S. Varol, F. C. Huang, K. L. Buehne, N. R. Mayne, I. Weitzhandler, M. Bonn, S. H. Parekh, A. Chilkoti, Genetically encoded lipid–polypeptide hybrid biomaterials that exhibit temperature-triggered hierarchical self-assembly. *Nat. Chem.* **10**, 496–505 (2018).
21. A. Sorrenti, J. Leira-Iglesias, A. J. Markvoort, T. F. A. de Greef, T. M. Hermans, Non-equilibrium supramolecular polymerization. *Chem. Soc. Rev.* **46**, 5476–5490 (2017).
22. E. R. Wright, R. A. McMillan, A. Cooper, R. P. Apkarian, V. P. Conticello, Thermoplastic elastomer hydrogels via self-assembly of an elastin-mimetic triblock polypeptide. *Adv. Funct. Mater.* **12**, 149–154 (2002).
23. H. B. Schmidt, R. Rohatgi, In vivo formation of vacuolated multi-phase compartments lacking membranes. *Cell Rep.* **16**, 1228–1236 (2016).
24. J. Seuring, S. Agarwal, First example of a universal and cost-effective approach: Polymers with tunable upper critical solution temperature in water and electrolyte solution. *Macromolecules* **45**, 3910–3918 (2012).
25. T. Murakami, S. Qamar, J. Q. Lin, G. S. K. Schierle, E. Rees, A. Miyashita, A. R. Costa, R. B. Dodd, F. T. S. Chan, C. H. Michel, D. Kronenberg-Versteeg, Y. Li, S.-P. Yang, Y. Wakutani, W. Meadows, R. R. Ferry, L. Dong, G. G. Tartaglia, G. Favrin, W.-L. Lin, D. W. Dickson, M. Zhen, D. Ron, G. Schmitt-Ulms, P. E. Fraser, N. A. Shneider, C. Holt, M. Vendruscolo, C. F. Kaminski, P. St. George-Hyslop, ALS/FTD mutation-induced phase transition of FUS liquid droplets and reversible hydrogels into irreversible hydrogels impairs RNP granule function. *Neuron* **88**, 678–690 (2015).
26. Y. Shin, J. Berry, N. Pannucci, M. P. Haataja, J. E. Toettcher, C. P. Brangwynne, Spatiotemporal control of intracellular phase transitions using light-activated optoDroplets. *Cell* **168**, 159–171.e14 (2017).
27. M. J. Glassman, B. D. Olsen, Arrested phase separation of elastin-like polypeptide solutions yields stiff, thermoresponsive gels. *Biomacromolecules* **16**, 3762–3773 (2015).
28. J.-D. Pédelacq, S. Cabantous, T. Tran, T. C. Terwilliger, G. S. Waldo, Engineering and characterization of a superfolder green fluorescent protein. *Nat. Biotechnol.* **24**, 79–88 (2006).
29. L. B. Sagle, Y. Zhang, V. A. Litosh, X. Chen, Y. Cho, P. S. Cremer, Investigating the hydrogen-bonding model of urea denaturation. *J. Am. Chem. Soc.* **131**, 9304–9310 (2009).
30. N. K. Li, F. G. Quiroz, C. K. Hall, A. Chilkoti, Y. G. Yingling, Molecular description of the LCST behavior of an elastin-like polypeptide. *Biomacromolecules* **15**, 3522–3530 (2014).
31. S. Perticaroli, J. D. Nickels, G. Ehlers, A. P. Sokolov, Rigidity, secondary structure, and the universality of the boson peak in proteins. *Biophys. J.* **106**, 2667–2674 (2014).
32. S. L. Perry, L. Leon, K. Q. Hoffmann, M. J. Kade, D. Priftis, K. A. Black, D. Wong, R. A. Klein, C. F. Pierce III, K. O. Margossian, J. K. Whitmer, J. Qin, J. J. de Pablo, M. Tirrell, Chirality-selected phase behaviour in ionic polypeptide complexes. *Nat. Commun.* **6**, 6052 (2015).
33. Y. Maeda, T. Nakamura, I. Ikeda, Changes in the hydration states of poly(*N*-*n*-propylmethacrylamide) and poly(*N*-isopropylmethacrylamide) during their phase transitions in water observed by FTIR spectroscopy. *Macromolecules* **34**, 8246–8251 (2001).
34. B. Jeong, S. W. Kim, Y. H. Bae, Thermosensitive sol–gel reversible hydrogels. *Adv. Drug Deliv. Rev.* **54**, 37–51 (2002).
35. J.-F. Lutz, M. Ouchi, D. R. Liu, M. Sawamoto, Sequence-controlled polymers. *Science* **341**, 1238149 (2013).
36. S. Rauscher, S. Baud, M. Miao, F. W. Keeley, R. Pomès, Proline and glycine control protein self-organization into elastomeric or amyloid fibrils. *Structure* **14**, 1667–1676 (2006).

37. N. K. Li, S. Roberts, F. G. Quiroz, A. Chilkoti, Y. G. Yingling, Sequence directionality dramatically affects LCST behavior of elastin-like polypeptides. *Biomacromolecules* **19**, 2496–2505 (2018).
38. M. R. Dreher, A. J. Simnick, K. Fischer, R. J. Smith, A. Patel, M. Schmidt, A. Chilkoti, Temperature triggered self-assembly of polypeptides into multivalent spherical micelles. *J. Am. Chem. Soc.* **130**, 687–694 (2008).
39. S. R. MacEwan, I. Weitzhandler, I. Hoffmann, J. Genzer, M. Gradzielski, A. Chilkoti, Phase behavior and self-assembly of perfectly sequence-defined and monodisperse multi-block copolypeptides. *Biomacromolecules* **18**, 599–609 (2017).
40. Y. Geng, P. Dalhaimer, S. Cai, R. Tsai, M. Tewari, T. Minko, D. E. Discher, Shape effects of filaments versus spherical particles in flow and drug delivery. *Nat. Nanotechnol.* **2**, 249–255 (2007).
41. C. Cai, J. Lin, Y. Lu, Q. Zhang, L. Wang, Polypeptide self-assemblies: Nanostructures and bioapplications. *Chem. Soc. Rev.* **45**, 5985–6012 (2016).
42. M. Amiram, F. G. Quiroz, D. J. Callahan, A. Chilkoti, A highly parallel method for synthesizing DNA repeats enables the discovery of 'smart'protein polymers. *Nat. Mater.* **10**, 141–148 (2011).
43. J. R. McDaniel, J. A. MacKay, F. G. Quiroz, A. Chilkoti, Recursive directional ligation by plasmid reconstruction allows rapid and seamless cloning of oligomeric genes. *Biomacromolecules* **11**, 944–952 (2010).
44. W. Hassouneh, S. R. MacEwan, A. Chilkoti, Fusions of elastin-like polypeptides to pharmaceutical proteins. *Meth. Enzymol.* **502**, 215–237 (2012).
45. N. J. Greenfield, Using circular dichroism spectra to estimate protein secondary structure. *Nat. Protoc.* **1**, 2876–2890 (2007).
46. D. A. Case, T. A. Darden, I. T.E. Cheatham, C. L. Simmerling, J. Wang, R. E. Duke, R. Luo, R. C. Walker, W. Zhang, K. M. Merz, B. Roberts, S. Hayik, A. Roitberg, G. Seabra, J. Swails, A. W. Goetz, I. Kolossváry, K. F. Wong, F. Paesani, J. Vanicek, R. M. Wolf, J. Liu, X. Wu, S. R. Brozell, T. Steinbrecher, H. Gohlke, Q. Cai, X. Ye, J. Wang, M.-J. Hsieh, G. Cui, D. R. Roe, D. H. Mathews, M. G. Seetin, R. Salomon-Ferrer, C. Sagui, V. Babin, T. Luchko, S. Gusarov, A. Kovalenko, P. A. Kollman, *AMBER 12* (University of California, San Francisco, 2012).
47. W. L. Jorgensen, J. Chandrasekhar, J. D. Madura, R. W. Impey, M. L. Klein, Comparison of simple potential functions for simulating liquid water. *J. Chem. Phys.* **79**, 926–935 (1983).
48. J. Shao, S. W. Tanner, N. Thompson, T. E. Cheatham, Clustering molecular dynamics trajectories: 1. Characterizing the performance of different clustering algorithms. *J. Chem. Theory Comput.* **3**, 2312–2334 (2007).
49. J. C. Phillips, R. Braun, W. Wang, J. Gumbart, E. Tajkhorshid, E. Villa, C. Chipot, R. D. Skeel, L. Kale, K. Schulten, Scalable molecular dynamics with NAMD. *J. Comput. Chem.* **26**, 1781–1802 (2005).
50. H. Yu, Y. Zhao, C. Guo, Y. Gan, H. Huang, The role of proline substitutions within flexible regions on thermostability of luciferase. *Biochim. Biophys. Acta Proteins Proteom.* **1854**, 65–72 (2015).
51. M. T. Ruggiero, J. Sibik, R. Orlando, J. A. Zeitler, T. M. Korter, Measuring the elasticity of poly-L-proline helices with terahertz spectroscopy. *Angew. Chem. Int. Ed.* **55**, 6877–6881 (2016).
52. A. Micsonai, F. Wien, L. Kernya, Y.-H. Lee, Y. Goto, M. Réfrégiers, J. Kardos, Accurate secondary structure prediction and fold recognition for circular dichroism spectroscopy. *Proc. Natl. Acad. Sci. U.S.A.* **112**, E3095–E3103 (2015).
53. N. K. Dutta, M. Y. Truong, S. Mayavan, N. R. Choudhury, C. M. Elvin, M. Kim, R. Knott, K. M. Nairn, A. J. Hill, A genetically engineered protein responsive to multiple stimuli. *Angew. Chem. Int. Ed.* **50**, 4428–4431 (2011).

Acknowledgments: F.G.Q. thanks P. Gainza (at EPFL) for useful discussions on protein structure, comments on the manuscript, and assistance with the study of sequence-reversed peptides. A.C. thanks colleagues at North Carolina State University (Carol Hall and Jan Genzer) for stimulating discussions. **Funding:** This work was funded by the NIH through grant no. R01 GM061232 and MIRA R35GM127042 to A.C., by the NSF through a DMREF grant (NSF-DMR-1729671) to A.C., and by the NSF through the Research Triangle MRSEC (NSF DMR-11-21107). F.G.Q. holds a Career Award at the Scientific Interface from BWF. **Author contributions:** F.G.Q. designed and performed experiments, analyzed data, and wrote the manuscript. N.K.L. and Y.G.Y. performed MD simulations, analyzed data, and wrote the manuscript. S.R. performed experiments and wrote the manuscript. I.W. performed preliminary Cryo-TEM imaging. M.D. and P.W. performed the Cryo-TEM work. A.C. designed experiments, analyzed data, and wrote the manuscript. **Competing interests:** A.C. and F.G.Q. are inventors on a patent related to this work filed by Duke University (no. 8,470,967, published 25 June 2013). The authors declare no other competing interests. **Data and materials availability:** All data needed to evaluate the conclusions in the paper are present in the paper and/or the Supplementary Materials. The plasmids encoding IDPPs can be provided by A.C. pending scientific review and a completed material transfer agreement. Requests for these materials should be submitted to ashutosh.chilkoti@duke.edu. Additional data related to this paper may be requested from the authors.

Submitted 2 April 2019
Accepted 26 September 2019
Published 18 October 2019
10.1126/sciadv.aax5177

Citation: F. G. Quiroz, N. K. Li, S. Roberts, P. Weber, M. Dzuricky, I. Weitzhandler, Y. G. Yingling, A. Chilkoti, Intrinsically disordered proteins access a range of hysteretic phase separation behaviors. *Sci. Adv.* **5**, eaax5177 (2019).